In Silico Demonstrations of the Impact of Wavelength and Skin Tone on Photoacoustic Breast Imaging

Guilherme S. P. Fernandes*† Theo Z. Pavan* and Muyinatu A. Lediju Bell†‡§
*Department of Physics, FFCLRP, University of Sao Paulo, Brazil
†Department of Electrical and Computer Engineering, Johns Hopkins University, Baltimore, MD, United States
‡Department of Biomedical Engineering, Johns Hopkins University, Baltimore, MD, United States
§Department of Computer Science, Johns Hopkins University, Baltimore, MD, United States

2023 IEEE International Ultrasonics Symposium (IUS) | 979-8-3503-4645-9/23/$31.00 ©2023 IEEE | DOI: 10.1109/IUS51837.2023.10307088

***Abstract*—Breast photoacoustic imaging is an emerging clinical application that requires non-invasive illumination through skin. However, the melanin content of skin can introduce unwanted acoustic clutter, thereby compromising target visibility and overall image quality, which presents a significant challenge when considering the wide range of skin tones that are expected to benefit from access to the technology. To quantify the impact of this challenge, we conducted a series of multidomain photoacoustic simulations using five optical wavelengths, 18 skin constitutive pigmentations, and a previously validated 3D breast model. Three scenarios were considered: (i) the baseline scenario, in which a photoacoustic target was surrounded by breast tissue and covered by a layer of skin; (ii) the baseline scenario with the skin layer removed; and (iii) the baseline scenario with the photoacoustic target removed. Clutter levels ranged -11 dB to 11 dB with the baseline scenario. When skin was removed, this clutter was reduced by up to 39 dB and the associated target contrast improved by up to 39 dB relative to the baseline scenario, confirming skin as the primary source of clutter. When the target was removed, clutter decreased by less than 2.7 dB relative to the baseline scenario, indicating minimal to nonexistent clutter contributions from scattering due to the presence of the photoacoustic target. Future work will investigate novel system designs and protocols for patient-specific photoacoustic imaging system customizations.**

I. Introduction

Breast cancer detection is an important, emerging clinical application of photoacoustic imaging, particularly after FDA premarket approval of a new breast photoacoustic imaging system design [1], [2]. However, non-invasive illumination through skin, which is a fundamental aspect of current breast photoacoustic imaging designs, presents a significant challenge when considering the variety of skin tones with potential clinical access to the technology. In particular, multiple *in vivo* studies indicate that the optical absorption of skin introduces pronounced acoustic clutter within photoacoustic images, deteriorating target visibility and reducing contrast and signal-to-noise ratios [3]–[6]. The optical absorption of skin is typically dominated by the presence of melanin within the epidermal layer [7]. As melanin is primarily responsible for skin pigmentation [8], a higher melanin concentration in darker skin tones corresponds to increased optical absorption by the skin, ultimately resulting in degraded image quality. For this reason, it is critical to comprehensively understand the sources of clutter generation from different skin tones, as this understanding is essential to establishing equitable photoacoustic imaging system designs and appropriate imaging protocols.

The individual typology angle (ITA°) provides an objective method to categorize skin tones. This classification is achieved by calculating ITA° using the L^* and b^* values from a colorimetric analysis based on the CIELAB color space [9]. Based on previous reports [9], [10], an individual's ITA° value can be used to categorize skin tone as follows: very light ($>55°$); light ($55° - 41°$); intermediate ($41° - 28°$); tan ($28° - 10°$); brown ($10° - 30°$); and dark ($<$ -30°). Notably, ITA° correlates directly with skin melanin content [11], and the equation proposed by Junior *et al.* [12] establishes a relationship between skin optical absorption coefficient, ITA°, and optical wavelength, which further demonstrates the practical utility of ITA°.

While it is understandably not possible to control all possible parameters of interest in a purely experimental setting, simulations do not suffer from this challenge. In addition, simulations enable us to quantify the impact of melanin on image quality and photoacoustic target visualization under a range of imaging scenarios. Therefore, we employ a previously validated 3D realistic breast model [13] to implement multidomain photoacoustic simulations with a representative range of controlled optical wavelengths and skin tones.

II. Materials and Methods

Multidomain photoacoustic simulations were performed by computing both light transport and acoustic wave propagation in a pre-defined volume of interest using the MCXLAB [14] and k-Wave [15] MATLAB (Natick, MA) toolboxes, respectively. Our simulated volume was based on a 3D realistic breast model [13], immersed in water, with one slice of this volume illustrated in Fig. 1. The dimensions of this volume were 40 mm x 15 mm x 20 mm in the lateral, axial, and longitudinal directions, respectively, with a voxel size of 100 μm. Within this volume, a spherical inclusion with a diameter of 3 mm was incorporated to represent a photoacoustic target. The optical

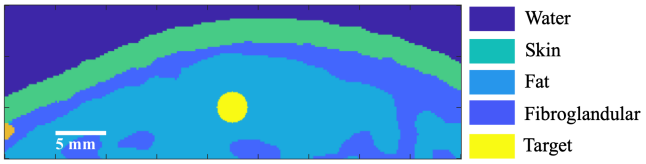

Fig. 1. A cross-sectional view of the simulated volume within the imaging plane, demonstrating various tissue constituents, including, water, skin, fat, fibroglandular tissue, and a photoacoustic target.

and acoustic properties of the target were configured to match those of blood.

For the optical component of the simulations, 10^8 photons were emitted using a 4-mm-radius collimated Gaussian beam, centrally positioned at the uppermost part of the volume. To evaluate the impact of wavelength and skin tone on the resulting photoacoustic images, a total of five wavelengths (532 nm, 750 nm, 810 nm, 870 nm, and 1064 nm) and 18 ITA° values (i.e., 3 samples from each skin tone category) were modeled. Reported values for the optical absorption coefficients of water [16], blood [16], fat [13], and fibroglandular tissue [13] were additionally modeled. The optical absorption coefficients for skin were calculated using the equation proposed by Junior *et al.* [12]. The optical scattering coefficients for all tissues were obtained from [7], and the anisotropy factor and index of refraction of all tissues were standardized to 0.9 and 1.37, respectively.

For the acoustic component of the simulations, the initial pressure was determined by considering the product $\Phi(\vec{r}) \cdot \mu_a(\vec{r})$, where $\Phi(\vec{r})$ is the output light fluence map derived from the optical simulation and $\mu_a(\vec{r})$ corresponds to the known optical absorption coefficient map used in the optical simulations. A linear array ultrasound transducer with 128 elements, 0.3 mm pitch, and a center frequency of 7 MHz was positioned at the top of the central slice to record the acoustic pressure. Table I summarizes the acoustic properties of each tissue component in the simulations.

To determine the magnitude, impact, and source of empirically observed clutter, three comparative scenarios were evaluated: (i) baseline, defined as a target surrounded by breast tissue with a skin layer present, (ii) baseline with the skin layer removed, and (iii) baseline with the target removed. Amplitude-based beamforming using a single-step fast Fourier transform (FFT) reconstruction technique [15] was applied using the k-Wave MATLAB toolbox to create the final images.

TABLE I
ACOUSTIC PROPERTIES

Layer	Speed of sound [m/s]	Density [kg/m^3]	Attenuation [dB/MHz·cm]
Water	1500	1000	0.0025
Skin	1650	1150	0.35
Fibroglandular	1515	1040	0.75
Fat	1470	937	0.60
Target	1584	1040	0.20

To quantify the observations, skin photoacoustic signal, clutter level, and target contrast were calculated as functions of wavelength (i.e., λ) and skin tone (i.e., ITA°) as follows:

$$\text{Skin signal}(\lambda, \text{ITA}^\circ) = 20 \cdot \log_{10}\left(\frac{s_{\text{skin}_{\lambda,\text{ITA}^\circ}}}{s_{\text{target}_{\lambda,\text{ITA}^\circ}}}\right), \quad (1)$$

$$\text{Clutter level}(\lambda, \text{ITA}^\circ) = 20 \cdot \log_{10}\left(\frac{s_{\text{clutter}_{\lambda,\text{ITA}^\circ}}}{s_{\text{target}_{\lambda,\text{ITA}^\circ}}}\right), \quad (2)$$

$$\text{Contrast}(\lambda, \text{ITA}^\circ) = 20 \cdot \log_{10}\left(\frac{s_{\text{target}_{\lambda,\text{ITA}^\circ}}}{s_{\text{clutter}_{\lambda,\text{ITA}^\circ}}}\right), \quad (3)$$

where $s_{\text{skin}_{\lambda,\text{ITA}^\circ}}$, $s_{\text{target}_{\lambda,\text{ITA}^\circ}}$ and $s_{\text{clutter}_{\lambda,\text{ITA}^\circ}}$ are the signal amplitudes averaged over regions of interest (ROIs) within the skin, the target, and an anticipated clutter-containing region underneath the skin, respectively. These ROIs were selected once using the image created with 750 nm wavelength and 60° ITA° (i.e., classified as very light skin tone), and the same ROIs were utilized for the remaining wavelengths and ITA° values.

III. Results

Fig. 2 shows representative examples of photoacoustic images produced by the baseline scenario for each optical wavelength and skin tone investigated, as well as corresponding examples with skin removed. When illuminated with 532 nm wavelength, the optical absorption of skin at this wavelength resulted in high-amplitude skin signals and poor target visibility. With longer wavelengths (i.e., 750 nm to 870 nm), the skin signal was lower and target visibility improved, due to the decrease in skin optical absorption, resulting in higher optical fluence throughout the imaging plane. However, the 1064 nm wavelength produced the lowest target visibility among the wavelengths investigated, because of the decrease in light fluence due to the elevated optical absorption of the initial layer of water, coupled with the low optical absorption of the target at this wavelength. When the skin layer was removed, the presence of acoustic clutter was qualitatively minimal to non-existent, and target visibility generally increased, which confirms skin as a predominant source of acoustic clutter.

Figs. 3(a), 3(b), and 3(c) quantify our observations of skin photoacoustic signal, clutter level, and target contrast, respectively, as functions of ITA° for the five wavelengths and three scenarios investigated. As expected for the baseline scenario, in Fig. 3(a), the skin photoacoustic signal decreased with increasing ITA° (i.e., with lighter skin tones) when illuminated with 532 nm to 870 nm wavelengths and was relatively constant as a function of ITA° values when illuminated with 1064 nm for the reasons stated above (i.e., primarily due to the optical absorption of water).

In Fig. 3(b), clutter generally decreased with an increase in ITA° and wavelength, as expected, with the exception of 1064 nm for the reasons stated above. When skin was removed, clutter further decreased by up to 39 dB, 27 dB, 28 dB, 23 dB, and 14 dB for the 532-, 750-, 810-, 870- and 1064-nm

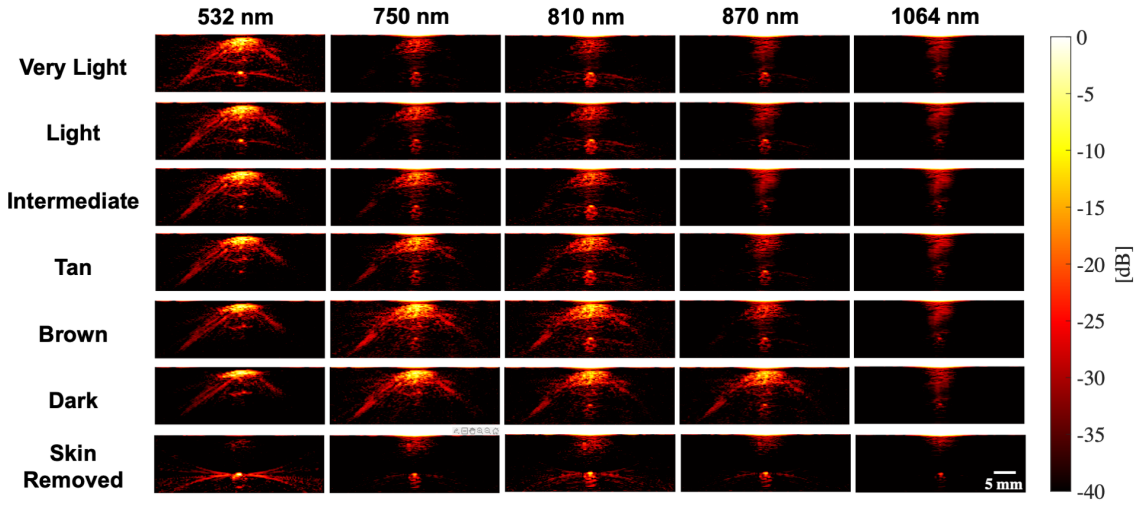

Fig. 2. Representative examples of photoacoustic images obtained with the multidomain simulations.

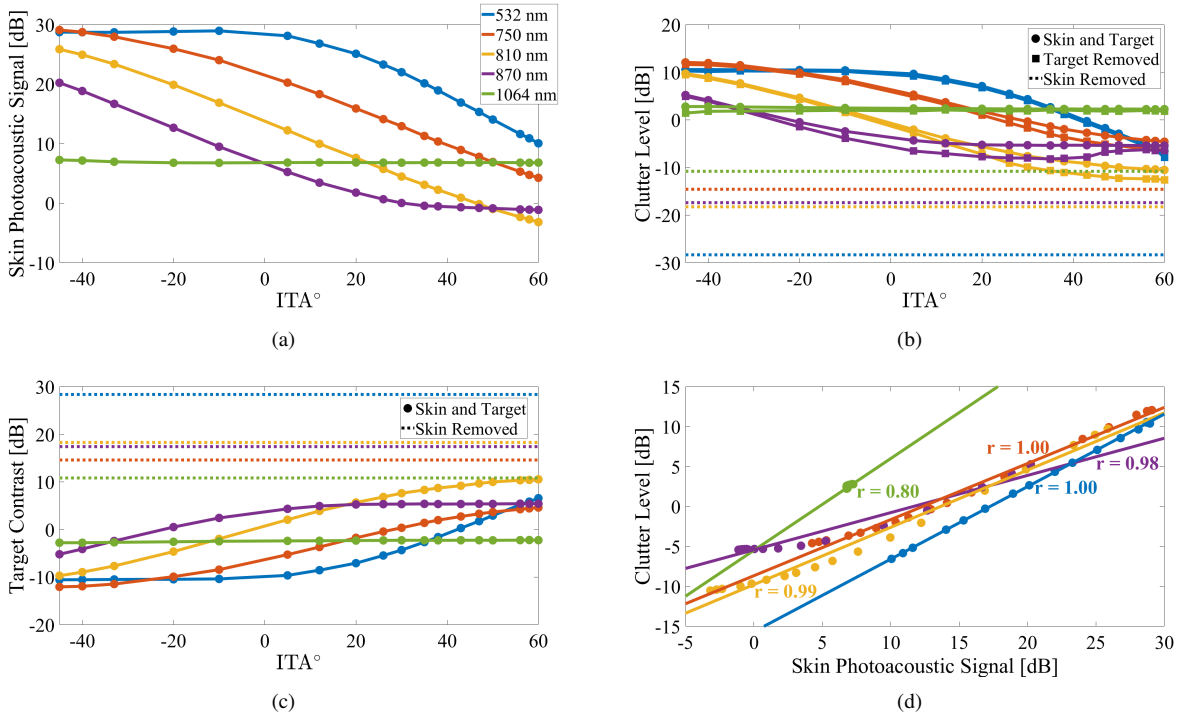

Fig. 3. (a) Skin photoacoustic signal as a function of ITA° for the baseline scenario. (b) Clutter level and (c) target contrast as functions of ITA° for the three scenarios investigated. (d) Clutter as a function of skin photoacoustic signal with r values representing the correlation of these two variables for each optical wavelength described in the legend of (a).

wavelengths, respectively, when compared to the clutter levels for each baseline scenario. When the target was removed, clutter decreased by less than 2.7 dB relative to the baseline scenario for each wavelength and skin tone investigated, indicating minimal to nonexistent clutter contributions from any possible scattering caused by the presence of the simulated photoacoustic target.

In Fig. 3(c), target contrast generally increased with increasing ITA° (i.e., lighter skin tones), with the exception of the 1064 nm wavelength, due to the impact of the water layer as described above. When skin was removed, the contrast improved by up to 39 dB, 27 dB, 28 dB, 23 dB, and 14 dB for the 532-, 750-, 810-, 870- and 1064-nm wavelengths, respectively, when compared to the contrast for each baseline scenario.

Fig. 3(d) quantifies clutter as a function of the corresponding skin photoacoustic signal for each wavelength investigated. This result demonstrates the correlation between these vari-

ables when imaging with wavelengths ranging 532 nm to 870 nm. This correlation was lower when imaging with a wavelength of 1064 nm, further highlighting the water layer as responsible for the observed clutter with this wavelength.

IV. Discussion

Our qualitative and quantitative results highlight skin as the predominant source of acoustic clutter in non-invasive breast photoacoustic images. This observation is supported by both qualitative observations (Fig. 2) and the associated quantitative clutter reduction (Fig. 3(b)) and target contrast increase (Fig. 3(c)), observed after the removal of skin. We are aware that the reported clutter reduction with the 1064 nm wavelength may seem counterintuitive because the associated clutter primarily originated from the water layer. However, the related clutter reduction achieved in the absence of skin suggests that the presence of skin increases the acoustic impedance mismatch between the water layer and breast tissue, thus increasing the level of clutter in the associated photoacoustic images.

Our results are additionally insightful with respect to appropriate wavelengths to utilize in photoacoustic breast imaging. In particular, illumination and visualization of contents within a photoacoustic target is critical when imaging a suspected tumor, as associated vascularization can be characterized to assist with a diagnosis [17], [18]. The optical absorption of blood is greatest with the 532 nm wavelength when compared to the other wavelengths included in this study (e.g., 23.5 mm^{-1} and 0.5 mm^{-1} for 532 nm and 1064 nm, respectively). Therefore, when the target is illuminated with 532 nm, the elevated optical absorption at the target surface appears to rapidly decrease the light fluence inside the target, resulting in a strong photoacoustic signal from the target boundary and a minimal signal inside the target (Fig. 2). As a result, target vascularization characterization is not expected to be possible when illuminating with 532 nm wavelength. However, when utilizing 810 nm or 870 nm wavelength, the photoacoustic images presented acceptable visualization inside the target with most skin tones (Fig. 2).

V. Conclusions

This work is the first to perform multidomain photoacoustic simulations using a realistic breast model with associated photoacoustic image visualizations. Quantitative and qualitative results demonstrate that skin is primarily responsible for the acoustic clutter and degraded target contrast observed within non-invasive photoacoustic images when utilizing multiple optical wavelengths. With the consistent presence of clutter across multiple wavelengths, it is unlikely that photoacoustic image quality can be overcome by simply altering the optical wavelength. Therefore, alternative system designs and advanced technological efforts (e.g., nonlinear beamforming and signal processing techniques) are necessary to reduce the observed skin tone bias, establish equitable photoacoustic imaging system designs, and define acceptable imaging protocols.

VI. Acknowledgements

This study was supported by Fundação de Amparo à Pesquisa do Estado de São Paulo (FAPESP) under Grants 2013/18854-6, 2017/14482-8, and 2022/01420-2. M.A.L.B. acknowledges grant number 2022-309513 from the Chan Zuckerberg Initiative DAF, an advised fund of Silicon Valley Community Foundation, and the National Institutes of Health (NIH) R01 EB032960 for partial support of her time on this project.

References

[1] A. Oraevsky, B. Clingman, J. Zalev, A. Stavros, W. Yang, and J. Parikh, "Clinical optoacoustic imaging combined with ultrasound for coregistered functional and anatomical mapping of breast tumors," *Photoacoustics*, vol. 12, pp. 30–45, 2018.

[2] "Premarket Approval (PMA) — accessdata.fda.gov." https://www.accessdata.fda.gov/scripts/cdrh/cfdocs/cfpma/pma.cfm?id=P200003. [Accessed 11-08-2023].

[3] G. S. P. Fernandes, J. H. Uliana, L. Bachmann, A. A. O. Carneiro, M. A. L. Bell, and T. Z. Pavan, "Impact of skin pigmentation on photoacoustic imaging using linear array transducer: a pilot in vivo study," in *2022 IEEE International Ultrasonics Symposium (IUS)*, pp. 1–4, IEEE, 2022.

[4] Y. Mantri and J. V. Jokerst, "Impact of skin tone on photoacoustic oximetry and tools to minimize bias," *Biomedical Optics Express*, vol. 13, no. 2, pp. 875–887, 2022.

[5] X. Li, U. Dinish, J. Aguirre, R. Bi, K. Dev, A. B. E. Attia, S. Nitkunanantharajah, Q. H. Lim, M. Schwarz, Y. W. Yew, *et al.*, "Optoacoustic mesoscopy analysis and quantitative estimation of specific imaging metrics in Fitzpatrick skin phototypes II to V," *Journal of Biophotonics*, vol. 12, no. 9, p. e201800442, 2019.

[6] S. Preisser, G. Held, H. G. Akarçay, M. Jaeger, and M. Frenz, "Study of clutter origin in in-vivo epi-optoacoustic imaging of human forearms," *Journal of Optics*, vol. 18, no. 9, p. 094003, 2016.

[7] S. L. Jacques, "Optical properties of biological tissues: a review," *Physics in Medicine & Biology*, vol. 58, no. 11, p. R37, 2013.

[8] J. Y. Lin and D. E. Fisher, "Melanocyte biology and skin pigmentation," *Nature*, vol. 445, no. 7130, pp. 843–850, 2007.

[9] B. C. K. Ly, E. B. Dyer, J. L. Feig, A. L. Chien, and S. Del Bino, "Research techniques made simple: cutaneous colorimetry: a reliable technique for objective skin color measurement," *Journal of Investigative Dermatology*, vol. 140, no. 1, pp. 3–12, 2020.

[10] A. Chardon, I. Cretois, and C. Hourseau, "Skin colour typology and suntanning pathways," *International Journal of Cosmetic science*, vol. 13, no. 4, pp. 191–208, 1991.

[11] S. Del Bino, S. Ito, J. Sok, Y. Nakanishi, P. Bastien, K. Wakamatsu, and F. Bernerd, "Chemical analysis of constitutive pigmentation of human epidermis reveals constant eumelanin to pheomelanin ratio," *Pigment Cell & Melanoma Research*, vol. 28, no. 6, pp. 707–717, 2015.

[12] L. B. C. Junior, C. E. Girasol, P. S. Coltro, R. R. Guirro, and L. Bachmann, "Absorption and reduced scattering coefficient estimation in pigmented human skin tissue by experimental colorimetric fitting," *JOSA A*, vol. 40, no. 9, pp. 1680–1685, 2023.

[13] Y. Lou, W. Zhou, T. P. Matthews, C. M. Appleton, and M. A. Anastasio, "Generation of anatomically realistic numerical phantoms for photoacoustic and ultrasonic breast imaging," *Journal of Biomedical Optics*, vol. 22, no. 4, pp. 041015–041015, 2017.

[14] Q. Fang and D. A. Boas, "Monte Carlo simulation of photon migration in 3D turbid media accelerated by graphics processing units," *Optics Express*, vol. 17, no. 22, pp. 20178–20190, 2009.

[15] B. E. Treeby and B. T. Cox, "k-Wave: MATLAB toolbox for the simulation and reconstruction of photoacoustic wave fields," *Journal of Biomedical Optics*, vol. 15, no. 2, p. 021314, 2010.

[16] "Assorted Spectra — omlc.org." https://omlc.org/spectra/index.html. [Accessed 14-08-2023].

[17] J. Folkman, "Clinical applications of research on angiogenesis," *New England Journal of Medicine*, vol. 333, no. 26, pp. 1757–1763, 1995.

[18] Y. Matsumoto and M. Toi, "Photoacoustic imaging of breast cancer," in *Screening and Risk Reduction Strategies for Breast Cancer: Imaging Modality and Risk-Reduction Approaches*, pp. 177–186, Springer, 2023.